Postnatal Brain Growth Patterns in Pontocerebellar Hypoplasia

Tessa van Dijk[1,2] Peter Barth[3] Frank Baas[2] Liesbeth Reneman[4,*] Bwee Tien Poll-The[3,*]

[1] Department of Clinical Genetics, Academic Medical Center, Amsterdam University Medical Center, Amsterdam, The Netherlands
[2] Department of Clinical Genetics, Leiden University Medical Center, Leiden, The Netherlands
[3] Department of Pediatric Neurology, Academic Medical Center, Amsterdam University Medical Center, Amsterdam, The Netherlands
[4] Department of Radiology and Nuclear Medicine, Academic Medical Center, Amsterdam University Medical Center, Amsterdam, The Netherlands

Address for correspondence Tessa van Dijk, MD, PhD, Department of Clinical Genetics, Academic Medical Center, Amsterdam University Medical Center, Meibergdreef 9, 1105 AZ Amsterdam, The Netherlands (e-mail: t.vandijk@amsterdamumc.nl).

Neuropediatrics 2021;52:163–169.

Abstract

Background Pontocerebellar hypoplasia (PCH) is a rare group of disorders mainly affecting the cerebellum and pons. Supratentorial structures are variably involved. We assessed brain growth patterns in patients with the most frequent forms of PCH, namely PCH1B (OMIM#614678) and PCH2A (OMIM#277470), since in these types of PCH, pre- and postnatal neurodegeneration is established by neuropathological profiling. To assess the influence of the different pathomechanisms on postnatal growth patterns, we included *CASK*-associated microcephaly and PCH (MICPCH, OMIM#300749) patients in our analyses, as MICPH mimics PCH on magnetic resonance imaging (MRI) but represents a developmental disorder including abnormal neuronal migration.

Methods A total of 66 patients were included: 9 patients with PCH1B, 18 patients with PCH2A, 6 patients with MICPCH, and 33 age- and gender-matched hospital-based controls. Segmentation of the vermis and cerebellum was performed manually, as were measurements of the thickness of the head of the caudate nucleus, the width of the anterior horn, and lateral ventricle size.

Results The cerebellum was severely hypoplastic at birth in all patients, and postnatal growth was nearly absent. In patients with PCH1B/2A, we found relative sparing of the vermis compared with the cerebellar hemispheres. In addition, PCH1B and PCH2A cases demonstrated thinning of the head of the caudate nucleus, an associated increase in anterior horn width, and an increase in lateral ventricle size. None of these features were seen in the MICPCH group.

Conclusions Our findings confirm the progressive nature including caudate nucleus atrophy in PCH1B and PCH2A. In MICPCH, the relative sparing of supratentorial structures confirms its different pathomechanism.

Keywords
- pontocerebellar hypoplasia
- *CASK* mutations
- cerebellum
- pons
- caudate nucleus
- brain volumetry
- MRI

* *These authors share last authorship.*

received
May 28, 2020
accepted
July 31, 2020
published online
October 27, 2020

Georg Thieme Verlag KG,
Rüdigerstraße 14,
70469 Stuttgart, Germany

DOI https://doi.org/10.1055/s-0040-1716900.
ISSN 0174-304X.

Background

Pontocerebellar hypoplasia (PCH) is a rare group of autosomal recessive heterogeneous disorders with a prenatal onset. PCH is morphologically characterized by severe hypoplasia of the cerebellum and pons, with variable involvement of the supratentorial structures (►**Fig. 1**).[1] Based on clinical features and genetic findings, the current classification comprises 13 distinct PCH subtypes (PCH1–13). Central motor impairments, epileptic seizures, and severe intellectual disability are common findings. Progressive microcephaly is a feature in some types and, based on neuroimaging reports and neuropathological studies, is suggested to result from ongoing postnatal neurodegeneration.[2] However, systematic studies of postnatal brain development in PCH patients are scarce. In a rare disorder such as PCH, patient numbers are often too small to collect cohorts of substantial size. To compare genetic homogeneous groups of PCH patients, we focused on the most frequent types, PCH1B and PCH2A, to assess infratentorial as well as supratentorial brain growth patterns.

PCH1 is characterized by anterior horn degeneration in the spinal cord similar to spinal muscular atrophy with muscle weakness and hypotonia.[3] Four genes are associated with PCH1A–D: *VRK1*, *EXOSC3*, *EXOSC8*, and *EXOSC9*, respectively (OMIM # 607596, #614678, # 616081, and # 618065). Mutations in *EXOSC3* are identified in approximately 50% of PCH1 patients.[4,5] PCH2A (OMIM #277470), which is caused by homozygosity for the p.A307S mutation in the *TSEN54* gene, is the most prevalent of all types of PCH.[6] Clinical features of PCH2A are jitteriness and incoordination of sucking and swallowing in the neonatal period followed by a severe developmental delay, extrapyramidal (chorea, dystonia), and pyramidal symptoms.[7]

Another relatively frequent disorder with severe PCH is caused by de novo mutations in the *CASK* gene. This X-linked disorder, also referred to as microcephaly and PCH (MICPCH, OMIM #300749), can mimic PCH on magnetic resonance imaging (MRI) (►**Fig. 1**), but it also differs in several aspects. First, *CASK* mutations appear to affect neuronal migration and result in a neurodevelopmental (e.g., not neurodegenerative)

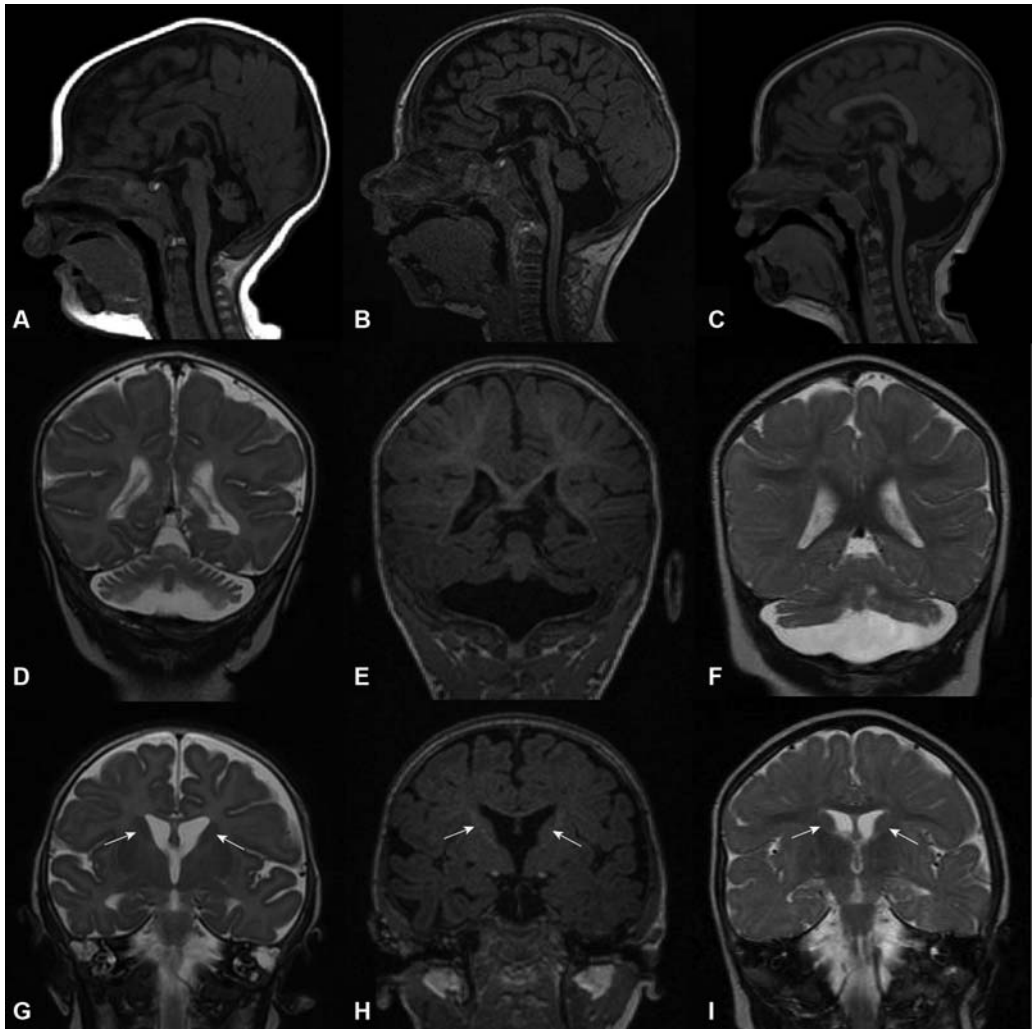

Fig. 1 MRIs (magnetic resonance imagings) of patients with pontocerebellar hypoplasia (PCH (1B), PCH2A, and microcephaly and PCH (MICPCH). (**A–C**) Midsagittal T1-weighted images of a patient with PCH1B, PCH2A, and MICPCH, respectively. Note loss of volume of the ventral pons and severe vermal hypoplasia in all three cases. (**D–I**) Coronal sections of PCH1B (**D,G**), PCH2A (**E,H**), and MICPCH (**F,I**) patients. Note relative sparing of the cerebellar vermis compared with the cerebellar hemispheres and flattening of the head of the caudate nucleus in PCH1B and PCH2A, but not in MICPCH. The caudate nucleus is indicated with a *yellow arrow*.

disorder.[8] Second, patients with MICPCH often have dysmorphic features, sensorineural hearing loss, or ophthalmologic abnormalities.[8–10]

Single time point MRI studies of PCH1B/2A patients and MICPCH patients are strikingly similar despite fundamental differences in presumed pathomechanism, for example, early degeneration (PCH1B, PCH2A) versus migration defect (MICPCH). However, these studies did not assess the growth rate of affected structures. Here, we compared postnatal brain growth patterns in patients with PCH1B/2A and MICPCH to assess the influence of the different pathomechanisms on disease progression. We hypothesized that enlargement of the lateral ventricles would be present in PCH1B and PCH2A as a result of ongoing neurodegeneration but not in MICPCH. Interestingly, thinning of the head of the caudate nucleus (CN) has been suggested in PCH1B and PCH2A, contributing to widening of the anterior horn of the lateral ventricle (►**Fig. 1G–H**).[5,11,12] Atrophy of the CN fits well with the prominent extrapyramidal movement disorders in PCH2A. We therefore also hypothesized that thinning of the CN would be most prominent in PCH2A.

Methods

Patients and MRI

Brain MRI scans from all patients with genetically proven PCH1B, PCH2A, or MICPCH were retrospectively collected from our in-house database. Patients up to 24 months of age were included. MR images were acquired in different hospitals within or outside the Netherlands. Informed consent was obtained through the referring clinicians.

In the PCH1A group, 9 patients with biallelic *EXOSC3* mutations met the inclusion criteria. The PCH2A group consisted of 18 patients, who were all homozygous for the p.A307S mutation in the *TSEN54* gene, and 6 patients with hetero- or hemizygous de novo mutations in the *CASK* gene were available. Patient and MRI characteristics are summarized in ►**Table 1**.

For each patient, a normal MRI of an age- and gender-matched hospital-based control was used. These MRIs were conducted for variable reasons (mainly seizures, anotia, head trauma). Prematurely born children were excluded from the control group. Sequence details of the controls are summarized in ►**Supplementary Table S1** (available online only).

MRI Analysis

Volumetric Measurements of Cerebellar Hemispheres and Vermis

We measured the volumes of the cerebellar hemispheres and vermis using the ITK-SNAP software.[13] Due to variability in quality and sequence details of the available scans, segmentation was done manually (►**Supplementary Fig. S1**; available online only). Volumes were measured in the sagittal plane, mostly in T1-weighted images, while the axial and coronal planes (if available) were used for orientation. Segmentation of the cerebellum was in line with previously described methods.[14–16]

Anterior Horn Width of the Lateral Ventricle and the Thickness of the Head of the Caudate Nucleus

The greatest anterior horn width (AHW) was measured mainly on T2-weighted images in the coronal plane at the level of the foramen of Monro.[17] The maximal thickness of the CN was measured in the same plane, if the inferior border of the CN could be properly distinguished from the internal capsule (►**Supplementary Fig. S2**; available online only).

Lateral Ventricle Area Index

The lateral ventricle area index (LVAI) was measured on T2-weighted images in the axial plane. First, the axial plane that showed the maximal area of the lateral ventricles was identified. The contours of the lateral ventricle were manually drawn, and the area was calculated using ITK-SNAP. The LVAI was calculated by dividing the maximal ventricular area by the corresponding total intradural area (►**Supplementary Fig. S3**; available online only).[18]

Validation

Intrarater variability was tested with the intraclass correlation coefficient (ICC) in randomly selected patients ($n = 10$). The mean ICC for the aforementioned measurements was 0.95.

Table 1 Overview of patient and MRI characteristics

Patient group	No. of patients	No. of males	Age range	Gene	High-resolution MRIs (≤1 mm)	High-resolution MRIs, controls (≤1 mm)
PCH1B	9	4	1d–6m	*EXOSC3*[a]	4	4
PCH2A	18	11	3d–14.8m	*TSEN54*[b]	4	7
MICPCH	6	2	2d–18.9m	*CASK*[c]	3	2

Abbreviations: d, days; m, months; MICPCH, microcephaly and pontocerebellar hypoplasia; MRI, magnetic resonance imaging; PCH, pontocerebellar hypoplasia.

[a]The following mutations in *EXOSC3* (NM_016042.3) were present in homozygous state: c.92G > C, p.(G31A) (5x), c.395A > C, p.(D132A), c.404G > A, p.(G135E). One patient was compound heterozygous for c.325T > A, p.(Y109N), and c.395A > C, p.(D132A); and one for c.325--4_329dupGTAGTATGT, p.(P111*), c.334G > A, p.(V112I), c.395A > C, and p.(D132A).

[b]All patients were homozygous for the c.919G > T, p.(A307S) mutation in *TSEN54* (NM_207346.2).

[c]All patients had de novo mutations in *CASK* (NM_003688.3): c.316C > T, p(K106*)(2x), c.670_674delGAAAG, p.(E224Ifs*3), c.1119_1131delins27, c.1915C > T, p.(K639*), c.1034del, p.(R345Kfsx24).

Data Analysis

The volumes of the cerebellar hemispheres and vermis were plotted against age, compiling cross-sectional growth curves. A linear regression model best fitted the data ($y = a + b^*x$), with age as the independent variable.

To quantify whether the cerebellar vermis was relatively spared in comparison to the cerebellar hemispheres, we calculated the cerebellar vermis:cerebellar hemisphere ratio. This ratio, as well as the LVAI, thickness of the head of the CN, and AHW, was compared between the PCH1B, PCH2A, and MICPCH patient groups and their corresponding control groups using the Mann–Whitney *U* test. Since every patient was coupled to an age- and gender-matched control, comparison between groups could be done without correction for age.

Results

Volume of the Cerebellar Vermis, Cerebellar Hemispheres, and Pons

In all patient groups, volumes of the cerebellar vermis and cerebellar hemispheres were already distinctly smaller at birth compared with the corresponding control groups. Also, the estimated yearly growth rate of these structures, which was based on the linear regression curves that best fitted the data, was considerably lower in the patient groups (►**Fig. 2A–F**; ►**Supplementary Table S2** [available online only]).

Ratio of Cerebellar Vermis to Cerebellar Hemispheres

The ratio of the volume of the cerebellar vermis to cerebellar hemispheres was significantly higher in PCH1B ($p = 0.019$; ►**Fig. 2G**) and PCH2A ($p < 0.0001$; ►**Fig. 2H**) when compared with controls. No difference was observed in the MICPCH patients compared with controls ($p = 0.589$; ►**Fig. 2I**).

Anterior Horn Width and Thickness of the Head of the Caudate Nucleus

The maximal thickness of the head of the CN at the foramen of Monro was significantly less in PCHB1 and PCH2A patients when compared with controls ($p = 0.002$ in the PCH1B group and $p < 0.001$ in the PCH2A group; ►**Fig. 3A, B**). In *CASK* patients, the thickness of the CN could only be reliably determined in four patients, and in this small group no significant

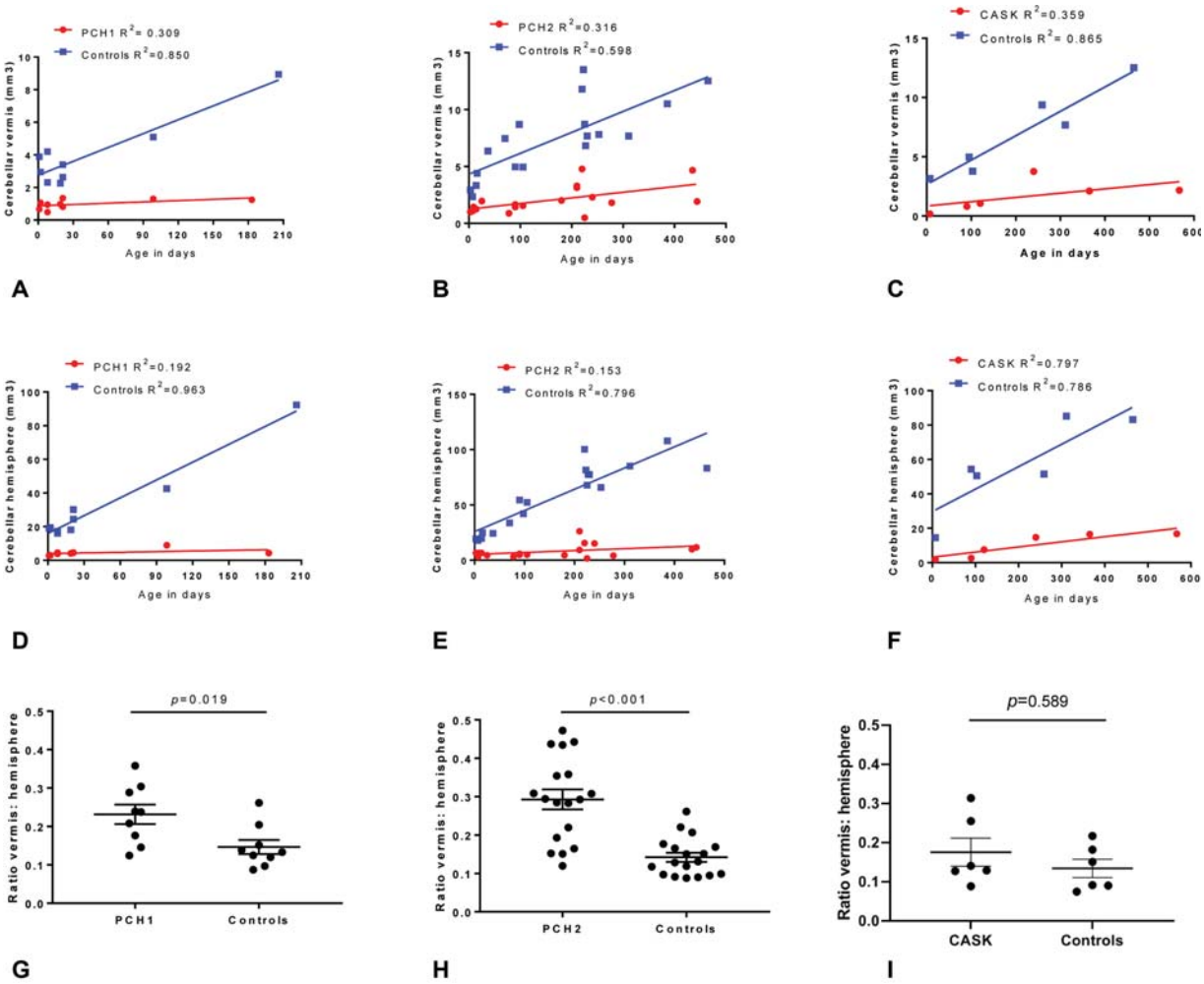

Fig. 2 Volumes of cerebellar vermis and hemispheres in pontocerebellar hypoplasia (PCH) 1, PCH2A, and *CASK* patients compared with controls, including the ratio of vermis to cerebellar hemisphere volume. Scatterplots showing cerebellar vermis volumes (**A–C**) and volumes of cerebellar hemispheres (**D–F**) in PCH1B, PCH2A, and *CASK* patients compared with controls. Size at birth and yearly growth rate predicted based on the linear regression curve that best fitted the data are depicted. (**G–I**) The ratio of vermis to cerebellar hemisphere volume in PCH1B, PCH2A, and *CASK* patients, plotted as mean ± standard error of the mean.

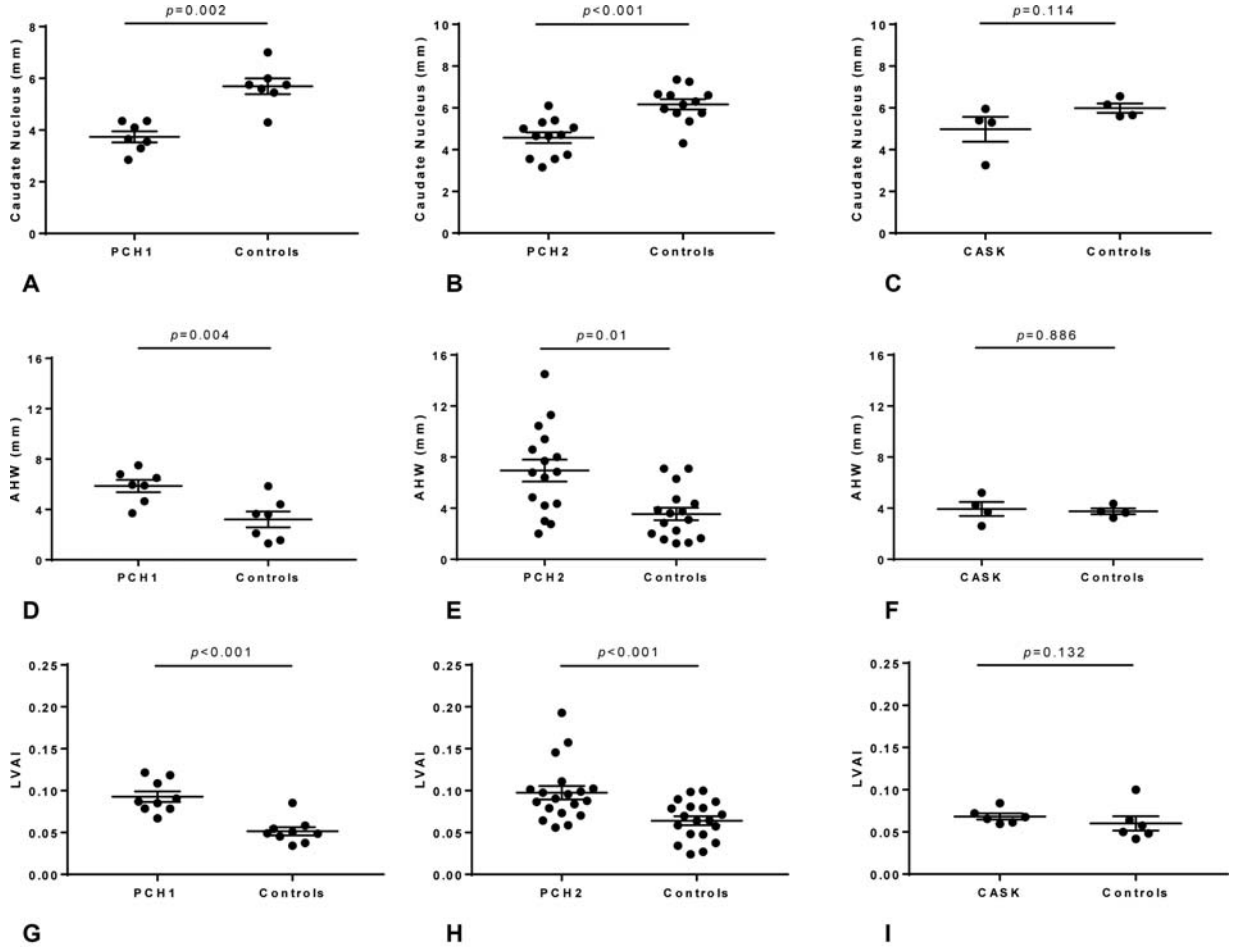

Fig. 3 Thickness of the caudate nucleus (CN), anterior horn width, and lateral ventricle area index in pontocerebellar hypoplasia (PCH) 1B, PCH2A, and *CASK* patients compared with controls. (**A**) Thickness of the CN in the PCH1B group compared with controls, plotted as mean ± standard error of the mean (SEM) ($p = 0.002$). (**B**) Thickness of the CN in PCH2A group compared with controls, plotted as mean ± SEM (***$p < 0.001$). (**C**) Thickness of the CN in *CASK* patients ($n = 4$) compared with controls, plotted as mean ± SEM ($p = 0.114$). (**D**) Anterior horn width (AHW) in the PCH1B group compared with controls, plotted as mean ± SEM ($p = 0.004$). (**E**) AHW in the PCH2A group compared with controls, plotted as mean ± SEM ($p = 0.01$). (**F**) AHW in *CASK* patients compared with controls, plotted as mean ± SEM ($p = 0.886$). (**G**) Lateral ventricle area index (LVAI) in the PCH1B group compared with controls, plotted as mean ± SEM ($p < 0.001$). (**H**) LVAI in the PCH2A group compared with controls, plotted as mean ± SEM ($p < 0.001$). (**I**) LVAI in *CASK* patients compared with controls, plotted as mean ± SEM ($p = 0.132$).

Table 2 Summary of MRI features in PCH1B, PCH2A, and MICPCH based on this study

	PCH1B	PCH2A	MICPCH
Pontocerebellar hypoplasia	+	+	+
↓ Growth rate cerebellum	+	+	+
Relative sparing cerebellar vermis	+	+	–
Thinning of the caudate nucleus	+	+	–
Enlarged lateral ventricles	+	+	–

difference could be detected ($p = 0.114$; ►**Fig. 3C**). In the same slice, the AHW was measured. In PCH1B and PCH2A patients, the AHW was significantly larger compared with controls ($p = 0.004$ and $p = 0.01$, respectively; ►**Fig. 3D, E**). The AHW was not significantly different in MICPCH patients compared with controls ($p = 0.886$; ►**Fig. 3F**).

Lateral Ventricle Area Index

To evaluate the extent of supratentorial involvement in PCH, we estimated the relative size of the lateral ventricles using the LVAI and compared these to the corresponding control groups (►**Fig. 3G–I**). In both PCH1B and PCH2A, the LVAI was significantly higher compared with the controls ($p < 0.001$). In the MICPCH group, no significant difference was detected ($p = 0.132$).

Discussion

In this study, we show that the postnatal cerebellar volume in patients with PCH1B, PCH2A, and MICPCH is clearly reduced at birth compared with controls. As expected, postnatal growth of these structures was very limited in all three patient groups. In addition, we found relative sparing of the vermis, thinning of the head of the CN, and increase of the AHW and LVAI in patients with PCH1B/2A but not in patients with MICPCH. (see ►**Table 2** for a summary of the results)

Atrophy of the CN was reported in neuropathological studies in PCH2A patients and repeatedly mentioned as a neuroradiological feature in PCH1B and PCH2A.[5,11,12] Thinning of the CN fits particularly well with the clinical phenotype of PCH2A, in which central motor involvement is prominent. In line with this, we found thinning of the CN and associated widening of the AHW in both PCH groups. However, widening of the AHW could also be a result of general widening of the ventricular system and is not specifically related to atrophy of the CN. The basal ganglia, of which the caudate nuclei are part, have an important role in the regulation of activity from the motor and premotor cortex and are involved in extrapyramidal movement disorders.[19,20] Possibly, dysfunction of the caudate nuclei explains the chorea and dystonia that is almost invariably present in PCH2A patients. Flattening of the CN is also seen in PCH1B, but the loss of spinal motor neurons could mask the central motor symptoms in this group of patients. Dystonia and chorea are rarely reported in MICPCH patients. Accordingly, we found no difference in the thickness of the caudate nuclei of MICPCH patients ($n = 4$) compared with controls.

Ventriculomegaly and progressive microcephaly occur in PCH1B/2A as a consequence of ongoing neurodegeneration. In MICPCH patients, progressive microcephaly is also a consistent feature, but the cerebral defects in this group are considered a result of a neuronal migration defect.[8] Consistent with this, we found an increased LVAI in PCH1B/2A patients but not in MICPCH patients.

Recently, it has been suggested that the progressive microcephaly in PCH2A does not result from atrophy but from reduced cerebral growth as a secondary effect of the severe cerebellar hypoplasia.[21] In support of this hypothesis, Ekert et al observed growth of the supratentorial brain in the first years of life in children with PCH2A, although the increase in volume was reduced to that observed in controls.[21] However, previous neuropathology studies in PCH2A reported atrophic and neurodegenerative features in the neocortex. In addition, our group showed that knockdown of *TSEN54* expression in zebrafish embryos with antisense morpholinos resulted in neuronal cell death at 24 hpf, implying a mechanism of early onset neurodegeneration in PCH2A.[22] In addition, it is unclear why supratentorial atrophy, if solely an effect of cerebellocerebral disruption, is not observed in other conditions with severe PCH, for example, early onset spinocerebellar ataxia.[23] Our data from this study, together with the results of zebrafish experiments and neuropathological reports describing neurodegenerative features in PCH2A, imply a mechanism of impaired growth accompanied by signs of neurodegeneration, predominantly affecting the cerebellum in PCH.

A limitation of this study is the small numbers of patients within each group, especially in the MICPCH group, although we have the largest cohort of PCH patients in the Netherlands. In addition, the retrospective multicenter study design of this study explains the heterogeneity of the MRI datasets. MRI scans were acquired on different scanners, and high-resolution scans were often lacking, creating partial volume effects. Therefore, segmentations were performed manually to obtain reliable and precise results as evidenced by the high intrarater variability.

Conclusions

In children with PCH1B, PCH2A, and MICPCH, the cerebellum is severely hypoplastic at birth and shows very limited postnatal growth. To our knowledge, this is the first report that objectified that relative sparing of the vermis is present in patients with PCH2A, and to a lesser degree in PCH1B, and not in patients with MICPCH. In addition, thinning of the CN and widening of the AHW are present in PCH1B and PCH2A patients, but not in MICPCH patients. We also observed an increase in lateral ventricle size in PCH1B and PCH2A patients, which is indicative of ongoing postnatal neurodegeneration in PCH. Although the number of patients with MICPCH analyzed in our study was small, we suggest that these macroscopic findings likely underlie different pathomechanisms on postnatal growth patterns: early degeneration in PCH1B, PCH2A versus migration defects in MICPCH.

Ethics Approval

The Medical Ethics Review Committee of the Academic Medical Center declared that an official approval of this study by the committee was not required.

Consent for Publication

Not applicable.

Availability of Data and Material

Data are available on request at the Academic Medical Center, Amsterdam, for researchers who meet the criteria for access to data that are confidential.

Authors' Contribution

T. V. D. performed the MRI segmentations and measurements under supervision of L. R.. T. V. D. drafted the manuscript. L. R., B. T. P. T., F. B., and P. B. were involved in study design. All authors critically revised the manuscript and approved the final version.

Funding

This work was supported by the Joshua Deeth Foundation.

Conflict of Interests

The authors declare that they have no competing interests.

Acknowledgments

We acknowledge Mar Rodríguez-Girondo for helpful advice on statistical analysis. We also thank Paul Groot for technical assistance.

References

1 Namavar Y, Barth PG, Poll-The BT, Baas F. Classification, diagnosis and potential mechanisms in pontocerebellar hypoplasia. Orphanet J Rare Dis 2011;6:50
2 Barth PG, Aronica E, de Vries L, et al. . Pontocerebellar hypoplasia type 2: a neuropathological update. Acta Neuropathol 2007;114 (04):373–386
3 Barth PG. Pontocerebellar hypoplasias. An overview of a group of inherited neurodegenerative disorders with fetal onset. Brain Dev 1993;15(06):411–422

4 Wan J, Yourshaw M, Mamsa H, et al. . Mutations in the RNA exosome component gene EXOSC3 cause pontocerebellar hypoplasia and spinal motor neuron degeneration. Nat Genet 2012;44 (06):704–708
5 Eggens VR, Barth PG, Niermeijer J-MF, et al. . EXOSC3 mutations in pontocerebellar hypoplasia type 1: novel mutations and genotype-phenotype correlations. Orphanet J Rare Dis 2014;9:23
6 Budde BS, Namavar Y, Barth PG, et al. . tRNA splicing endonuclease mutations cause pontocerebellar hypoplasia. Nat Genet 2008;40 (09):1113–1118
7 Namavar Y, Barth PG, Kasher PRPCH Consortium. , et al; . Clinical, neuroradiological and genetic findings in pontocerebellar hypoplasia. Brain 2011;134(Pt 1):143–156
8 Najm J, Horn D, Wimplinger I, et al. . Mutations of CASK cause an X-linked brain malformation phenotype with microcephaly and hypoplasia of the brainstem and cerebellum. Nat Genet 2008;40 (09):1065–1067
9 Burglen L, Chantot-Bastaraud S, Garel C, et al. . Spectrum of pontocerebellar hypoplasia in 13 girls and boys with CASK mutations: confirmation of a recognizable phenotype and first description of a male mosaic patient. Orphanet J Rare Dis 2012;7:18
10 Moog U, Bierhals T, Brand K, et al. . Phenotypic and molecular insights into CASK-related disorders in males. Orphanet J Rare Dis 2015;10:44
11 Rudnik-Schöneborn S, Barth PG, Zerres K. Pontocerebellar hypoplasia. Am J Med Genet C Semin Med Genet 2014;166C(02): 173–183
12 Barth PG, Vrensen GFJM, Uylings HBM, Oorthuys JWE, Stam FC. Inherited syndrome of microcephaly, dyskinesia and pontocerebellar hypoplasia: a systemic atrophy with early onset. J Neurol Sci 1990;97(01):25–42
13 Yushkevich PA, Piven J, Hazlett HC, et al. . User-guided 3D active contour segmentation of anatomical structures: significantly improved efficiency and reliability. Neuroimage 2006;31(03): 1116–1128
14 Gousias IS, Edwards AD, Rutherford MA, et al. . Magnetic resonance imaging of the newborn brain: manual segmentation of labelled atlases in term-born and preterm infants. Neuroimage 2012;62(03):1499–1509
15 Vatansever D, Kyriakopoulou V, Allsop JM, et al. . Multidimensional analysis of fetal posterior fossa in health and disease. Cerebellum 2013;12(05):632–644
16 Le Strange E, Saeed N, Cowan FM, Edwards AD, Rutherford MA. MR imaging quantification of cerebellar growth following hypoxic-ischemic injury to the neonatal brain. AJNR Am J Neuroradiol 2004;25(03):463–468
17 Brouwer MJ, de Vries LS, Groenendaal F, et al. . New reference values for the neonatal cerebral ventricles. Radiology 2012;262 (01):224–233
18 Schob S, Weiß A, Dieckow J, et al. . Correlations of ventricular enlargement with rheologically active surfactant proteins in cerebrospinal fluid. Front Aging Neurosci 2017;8:324
19 DeLong M, Wichmann T. Update on models of basal ganglia function and dysfunction. Parkinsonism Relat Disord 2009;15 (Suppl 3):S237–S240
20 Neychev VK, Gross RE, Lehéricy S, Hess EJ, Jinnah HA. The functional neuroanatomy of dystonia. Neurobiol Dis 2011;42 (02):185–201
21 Ekert K, Groeschel S, Sánchez-Albisua I, et al. . Brain morphometry in pontocerebellar hypoplasia type 2. Orphanet J Rare Dis 2016;11 (01):100
22 Kasher PR, Namavar Y, van Tijn P, et al. . Impairment of the tRNA-splicing endonuclease subunit 54 (tsen54) gene causes neurological abnormalities and larval death in zebrafish models of pontocerebellar hypoplasia. Hum Mol Genet 2011;20(08):1574–1584
23 van Dijk T, Barth P, Reneman L, Appelhof B, Baas F, Poll-The BT. A de novo missense mutation in the inositol 1,4,5-triphosphate receptor type 1 gene causing severe pontine and cerebellar hypoplasia: Expanding the phenotype of ITPR1-related spinocerebellar ataxia's. Am J Med Genet A 2017;173(01):207–212